



Article

# Development of a CO<sub>2</sub> Sensor for Extracorporeal Life Support Applications

Michele Bellancini <sup>1,2</sup>, Laura Cercenelli <sup>3,\*</sup> , Stefano Severi <sup>1</sup> , Guido Comai <sup>2</sup> and Emanuela Marcelli <sup>3</sup>

<sup>1</sup> Department of Electrical, Electronic and Information Engineering “Guglielmo Marconi” (DEI), Alma Mater Studiorum University of Bologna, 40136 Bologna, Italy; michele.bellancini2@unibo.it (M.B.); stefano.severi@unibo.it (S.S.)

<sup>2</sup> MediCon Ingegneria s.r.l, 40054 Budrio, Italy; guido.comai@mediconingegneria.it

<sup>3</sup> Laboratory of Bioengineering, Department of Experimental Diagnostic and Specialty Medicine (DIMES), Alma Mater Studiorum University of Bologna, 40138 Bologna, Italy; emanuela.marcelli@unibo.it

\* Correspondence: laura.cercenelli@unibo.it

Received: 29 May 2020; Accepted: 25 June 2020; Published: 27 June 2020



**Abstract:** Measurement of carbon dioxide (CO<sub>2</sub>) in medical applications is a well-established method for monitoring patient’s pulmonary function in a noninvasive way widely used in emergency, intensive care, and during anesthesia. Even in extracorporeal-life support applications, such as Extracorporeal Carbon Dioxide Removal (ECCO<sub>2</sub>R), Extracorporeal Membrane Oxygenation (ECMO), and cardiopulmonary by-pass (CPB), measurement of the CO<sub>2</sub> concentration in the membrane oxygenator exhaust gas is proven to be useful to evaluate the treatment progress as well as the performance of the membrane oxygenator. In this paper, we present a new optical sensor specifically designed for the measurement of CO<sub>2</sub> concentration in oxygenator exhaust gas. Further, the developed sensor allows measurement of the gas flow applied to the membrane oxygenator as well as the estimation of the CO<sub>2</sub> removal rate. A heating module is implemented within the sensor to avoid water vapor condensation. Effects of temperature on the sensor optical elements of the sensors are disclosed, as well as a method to avoid signal–temperature dependency. The newly developed sensor has been tested and compared against a reference device routinely used in clinical practice in both laboratory and in vivo conditions. Results show that sensor accuracy fulfills the requirements of the ISO standard, and that is suitable for clinical applications.

**Keywords:** CO<sub>2</sub> Sensor; mid-IR; extracorporeal life support devices

## 1. Introduction

Capnometry is the measurement of carbon dioxide (CO<sub>2</sub>) concentration in respiratory gases [1]. It is a well-known and established method for monitoring patient’s pulmonary function in a noninvasive way, widely used in emergency situations, as well as in intensive care or during anesthesia [2–5]. Even if the traditional use of capnometry is related to the field of respiratory monitoring, the application of this measurement in extracorporeal life support (ECLS) systems such as Cardio-Pulmonary Bypass (CPB) [6], Extracorporeal Membrane Oxygenation (ECMO) [7], and Extracorporeal Carbon Dioxide Removal (ECCO<sub>2</sub>R) [8] has been proposed. The goal of these procedures is to add oxygen (O<sub>2</sub>) and remove carbon dioxide (CO<sub>2</sub>) from patient blood, which is pumped through a membrane oxygenator (MO) where, gas exchange between the blood and sweep gas in the MO takes place. Therefore, the measurement of CO<sub>2</sub> removed by the MO can be achieved placing a capnometer (CO<sub>2</sub> sensor) at the exhaust port of the MO. This method is called oxygenator exhaust capnometry. All the procedures mentioned above represent complex systems that require

strict monitoring of both patient and device conditions. In particular, monitoring of MO performance is crucial during extracorporeal circulation procedures, as it might indicate a functional impairment due to clot formation within the MO and therefore the need for MO replacement. In this context, the analysis of CO<sub>2</sub> concentration in the MO exhaust can be exploited to evaluate the so-called dead space, i.e., the portion of the MO that is ventilated, but not perfused by blood, and therefore not participating in gas exchange [7]. During ECMO procedure, monitoring of MO performance may provide information regarding both the patient's lung status and the MO contribution to the global ventilation, therefore guiding the weaning process [9]. In CPB procedures, the oxygenator exhaust capnometry has been proven to be a useful tool for continuously estimating the CO<sub>2</sub> concentration in arterial blood (P<sub>a</sub>CO<sub>2</sub>) in a noninvasive way, representing an alternative to gas blood analysis [10]. Further, variation in P<sub>a</sub>CO<sub>2</sub> during ECMO procedures is proven to be associated with higher mortality, due to the dangerous effect of high CO<sub>2</sub> level to brain circulation [11]. In ECCO<sub>2</sub>R, which is a procedure for treatment of hypercapnia (i.e., a condition of abnormally elevated CO<sub>2</sub> level in the blood) [12], the measurement of CO<sub>2</sub> concentration in the exhaust gas and of CO<sub>2</sub> removal rate represents a key parameter to estimate the treatment progress. Therefore, CO<sub>2</sub> monitoring in the exhaust gas of a MO is a useful tool for monitoring patient's status and MO conditions as well as for evaluating the progress of the extracorporeal procedure. In the ECLS context, a flow sensor can be used to gather information of sweep gas flow (GF). Combining the information about GF and CO<sub>2</sub> concentration, the removal rate of CO<sub>2</sub> (VCO<sub>2</sub>) expressed as [mL/min] can be obtained, this value represents the volume of CO<sub>2</sub> removed over time. Further, measurement of GF can be used to detect a failure or a disconnection of the gas flow line in the MO. Despite its relative ease, the oxygenator exhaust capnometry is not routinely applied, as some practical issues remain unsolved in providing a reliable measurement of CO<sub>2</sub> removal from the patient. Even though several CO<sub>2</sub> sensors for medical applications are available, such as Masimo AB EMMA™ [13] and Medtronic Microcap™ [14], these are intended for respiratory monitoring and are not suitable for direct use in ECLS procedures. One of the main obstacles to CO<sub>2</sub> measurement at the exhaust port of a MO is the condensation of the water vapor contained in the gas exhaust on the optical elements of the CO<sub>2</sub> sensor. The water vapor condensation causes degradation of the signal acquired by the sensor and therefore an incorrect estimation of CO<sub>2</sub> concentration. This paper presents a newly developed sensing platform designed explicitly for ECLS application comprising a CO<sub>2</sub> sensor and a flow sensor. A solution to avoid condensation of the water vapor on the CO<sub>2</sub> sensing elements is described, as well as the accuracy of the CO<sub>2</sub> measurements provided by the new sensor in comparison with commercial devices and reference standard requirements.

## 2. Materials and Methods

### 2.1. State-of-the-Art on CO<sub>2</sub> Sensors

Optical-based sensors represent the state-of-the-art in the measurement of CO<sub>2</sub> concentration in gases [15]. These are typically based on infrared spectroscopy, a well-known technique that exploits the ability of molecules to absorb light at specific wavelengths related to vibration and rotation mechanisms of molecules [16]. The Bourger–Lambert–Beer Law describes the working principle of these sensors [17]:

$$dI = -\alpha(\lambda)cI_0dx \quad (1)$$

where  $I$  is the transmitted radiation intensity,  $I_0$  is the incident radiation intensity,  $c$  is the analyte concentration,  $\alpha(\lambda)$  is the analyte-specific absorption coefficient, and  $x$  represent the optical path length. The integral form of the Bourger–Lambert–Beer's Law,

$$I = I_0e^{-\alpha(\lambda)cx} \quad (2)$$

shows that it is possible to calculate the analyte concentration observing variation of the transmitted radiation  $I$ , as it represents attenuation of the incident radiation  $I_0$  once it has passed through the

optical path  $x$  containing an amount  $c$  of the analyte with absorption coefficient  $\alpha(\lambda)$ . In Equation (2) is highlighted that the absorption coefficient is a wavelength-dependent parameter, so to correctly exploit the absorption measurement principle is of paramount importance that the incident light has a spectrum that includes the absorption band of the analyte of interest. For  $\text{CO}_2$ , the incident light spectrum shall be in the mid-infrared (mid-IR) region (3–8  $\mu\text{m}$ ) as the principal absorption peak for carbon dioxide is located at 4.25  $\mu\text{m}$  [18]. Further, to obtain a direct measurement of the analyte of interest, no other compounds shall have absorption bands included on the incident light spectrum. Therefore, the whole composition of the oxygenator exhaust gas mixture has to be considered in order to develop an efficient  $\text{CO}_2$  sensor for ECLS applications. The exhaust gas of a membrane oxygenator during ECLS procedure contains a variable concentration of the following chemical species: Oxygen ( $\text{O}_2$ ), Nitrogen ( $\text{N}_2$ ), Carbon Dioxide ( $\text{CO}_2$ ), and water vapor. As infrared radiations are absorbed only by asymmetrical molecules, only  $\text{CO}_2$  and water vapor ( $\text{H}_2\text{O}$ ) have absorption bands in the mid-IR region. Absorption spectra of  $\text{CO}_2$  and  $\text{H}_2\text{O}$  obtained from the HITRAN database [19] are reported in Figure 1.

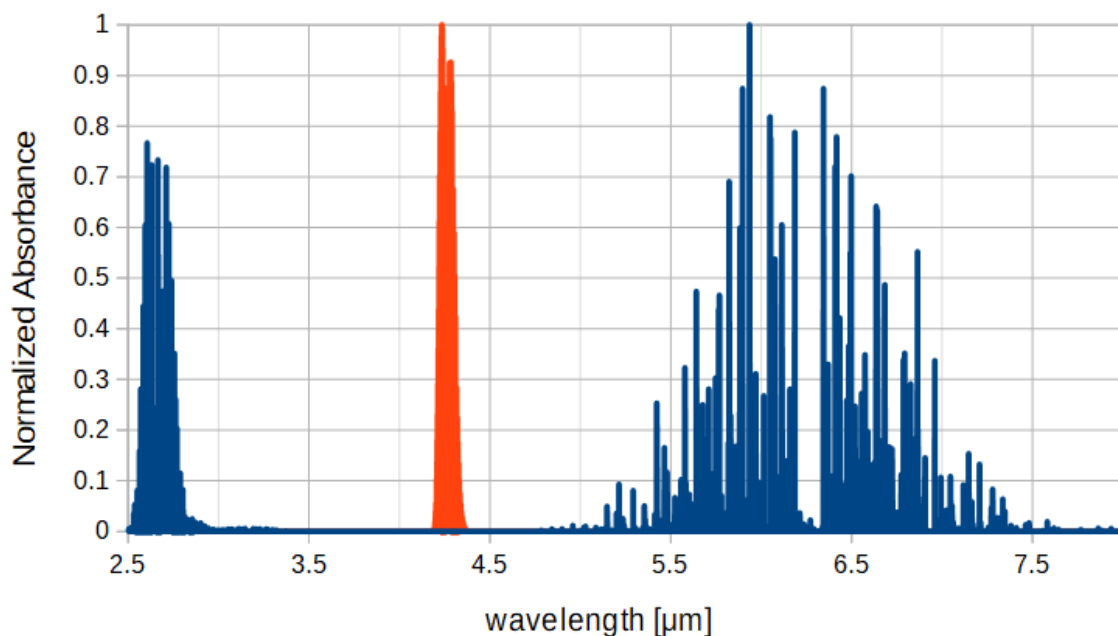


**Figure 1.** Absorption bands of  $\text{CO}_2$  (orange) and  $\text{H}_2\text{O}$  (blue) [19].

Methods to obtain emission in the mid-IR spectrum used in the currently available capnometers ( $\text{CO}_2$  sensors) involve the use of a broadband emitting incandescence light source coupled with thermopiles, pyroelectric detectors, or infrared photodiodes [20]. Use of a broadband emitting light source impose to add to the system a solution to filter the unwanted radiation, such as a beam splitter, optical filters, and a rotating filter wheel [21]. An alternative consists in the use of a narrow spectrum emitting diode coupled with an appropriate photodetector. This solution is possible thanks to the use of light-emitting diode (LED) and photodetector (PD) realized with InAsSb epitaxial layer on InAs substrate (InAsSb/InAs) [22]. Optical coupling of InAsSb/InAs LED and PD allows the emission and detection of IR radiation near 4.2  $\mu\text{m}$  that comprises the principal  $\text{CO}_2$  absorption peak, avoiding the use of mechanical modulators and interference filters and therefore allowing a simpler design of the sensor. Further, working in the region near 4.2  $\mu\text{m}$  allows the direct measurement of  $\text{CO}_2$  even in the presence of water vapor. In Figure 2, emission and detection spectra are shown. Note that, as LED and PD spectra overlap the  $\text{CO}_2$  absorption band, the measurement of  $\text{CO}_2$  concentration is possible.

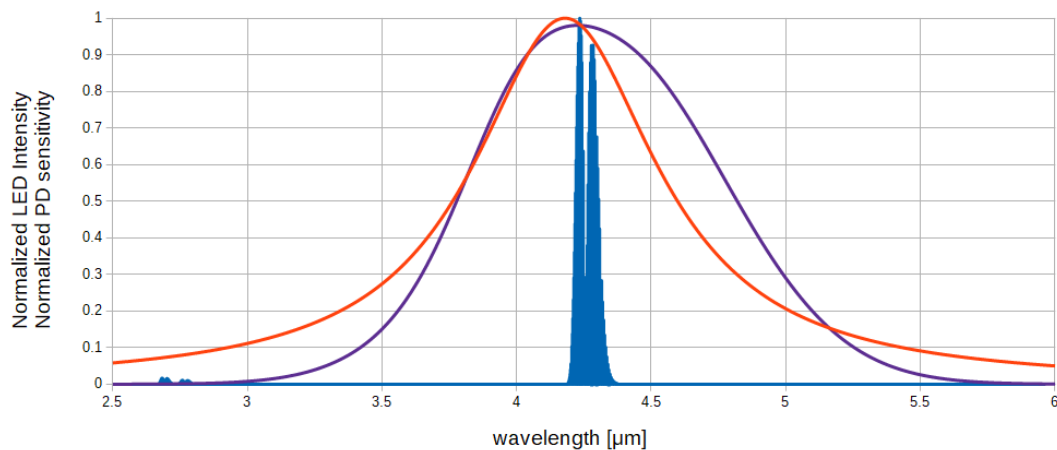


**Figure 2.** InAsSb/InAs LED (red) and PD (purple) spectra. CO<sub>2</sub> absorption band in the 4.2 μm region (blue) [19].

In commercially available optical CO<sub>2</sub> sensors for medical applications, two different approaches are used for measurement of CO<sub>2</sub> concentration: Main-stream and Side-stream [23]. In Main Stream sensors the measurement is taken on the main gas flow, using a measuring chamber that allows the emitted optical beam to cross the gas and to reach the detector, whereas in Side Stream sensors a portion of the gas flow is pulled by the sensors into a measurement chamber where the optical elements are positioned.

## 2.2. Design Requirements for CO<sub>2</sub> Sensors Applied to ECLS Procedures

Regarding the CO<sub>2</sub> sensor requirements intended for ECLS procedures, the following aspects shall be considered. First, a certain accuracy level is required for CO<sub>2</sub> measurement. Minimum accuracy for a CO<sub>2</sub> sensor in the medical field is defined by the standard ISO 80601-2-55 [24] as  $\pm 0.43\% + 8\%$  of the CO<sub>2</sub> concentration. A second aspect to take into account is that in ECLS procedures, the water vapor condensation at the exhaust port of the MO occurs, therefore the CO<sub>2</sub> sensor should implement a method to avoid the water vapor condensation on optical elements; otherwise, the optical signal deterioration due to condensation will lead to incorrect estimation of CO<sub>2</sub> concentration. Some capnometers for the measurement of CO<sub>2</sub> concentration in the exhaled breath, use a heating system to increase the temperature in the measuring chamber, avoiding water vapor condensation [25]. It is noteworthy that the effect of water vapor condensation is worse in ECLS procedures than in exhaled breath monitoring, due to the presence of a continuous gas flow and higher flow rate at the oxygenator exhaust port. Therefore, considering the water vapor condensation effect, in ECLS procedure a Main-stream CO<sub>2</sub> sensor is more appropriate than a Side-stream sensor, as in the latter, the water vapor can easily condensate in the tube used to bring the gas sample to the measuring chamber, thus leading to clotting of the sample line and compromising the correct measurement [26]. Further, the use of Side-stream CO<sub>2</sub> sensor at the oxygenator exhaust port has the drawback of the environmental air pulled to the measuring chamber together with the exhaust gas, which leads to the incorrect estimation of CO<sub>2</sub> removed from the patient [27]. An answer to this problem may consist in placement of the sampling tube inside the MO exhaust port [28]. This solution brings to sterilization issues that are not compatible with clinical routine in intensive care unit (ICU). An additional requirement that a CO<sub>2</sub> sensor for ECLS application should fulfill is the possibility to get the carbon dioxide removal rate VCO<sub>2</sub>. Therefore, a method to measure the gas flow (GF) applied to the MO should be implemented. Regarding time resolution of the obtained measurement, differently from respiratory capnometry in which high time resolution is necessary to obtain information on the end-tidal CO<sub>2</sub> and respiratory rate, capnometry applied to ECLS procedures, does not require such highly time-resolved measurement, as in ECLS applications the oxygenator exhaust gas flow and CO<sub>2</sub> concentration change slowly. Therefore, temporal resolution of the order of minutes is sufficient to extract information about

the ECLS procedure, that are used for evaluation of long-term therapy progress and trends. Finally, a CO<sub>2</sub> sensor for ECLS application should not be designed as a standalone device, but rather it should be interfaced with monitoring devices already used to monitor the patient's condition or to the ECLS device itself.

### 2.3. The Newly Developed CO<sub>2</sub> Sensing Platform

The proposed solution consists of a sensing platform made up of two sections: one for the GF measurement and the other one for CO<sub>2</sub> measurement, as illustrated in Figure 3. The flow measurement section contains an off-the-shelf mass flow sensor (SFM4100, Sensirion AG, Staefa, Switzerland) able to measure GF up to 20 SLM (Standard Litre per Minute) with accuracy of 3% on the measured value. As stated before, measurements taken at MO exhaust port are affected by water vapor condensation. Differently from the CO<sub>2</sub> sensor, increment of the sensor temperature is not a suitable solution to avoid water vapor condensation in the GF measurement section, as it would interfere with the measurement principle exploited by the flow sensor, that depends on the cooling effect applied by a gas flow on a heating element placed within the sensor [29]. Therefore, to avoid measurement error due to water vapor, the GF measurement section has been designed to be positioned at the inlet port of the MO. Further, measurement of GF at the inlet port of the MO provides to the operator a direct feedback about the sweep gas flow used for the extracorporeal procedure. Data collected by the flow sensor are communicated through I2C interface to the CPU contained in the CO<sub>2</sub> measurement section.

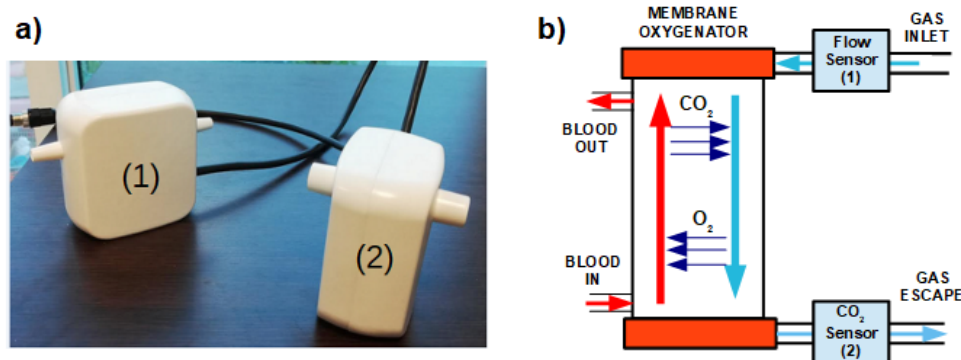


**Figure 3.** (a) Developed CO<sub>2</sub> sensing platform . (1) Flow measurement section; (2) CO<sub>2</sub> measurement section. (b) Schematic representation of flow sensor and CO<sub>2</sub> sensor on MO.

The CO<sub>2</sub> measurement section has been entirely developed and is made up by three subsections:

1. emission stage for the generation of the mid-IR beam;
2. receiver stage for the detection, conditioning and amplification of the optical signal after CO<sub>2</sub> absorption and;
3. CPU for signal acquisition, processing, and communication with a host device.

For both emission and detection of the mid-IR beam, optical elements of InAsSb/InAs (LED Microsensor NT, Saint-Petersburg, Russia) are used [30]. A parabolic reflector is mounted on both LED and PD to improve directivity of the mid-IR beam and therefore the optical coupling. LED and PD are placed on opposite sides of a measuring cuvette, and are mechanically fixed in order to assure the correct positioning and optimal optical coupling. To protect the optical elements, a sapphire glass window is mounted on the parabolic reflector. As only a single LED-PD couple is used, this solution represents a single-channel architecture. Use of the single-channel architecture allows to obtain a simpler device, easy to assemble and cheaper, as no optical filters or beam splitter are used. As InAsSb/InAs elements are affected by the variability in their optical performance in terms of emission efficiency and photosensitivity, the microcontroller can modulate the LED current and amplification gain of the receiver stage allowing the proper tuning of each optical couple in order to achieve the best

performance. Measuring chamber of the sensor has been designed to be connected directly to the MO exhaust port connector, therefore implementing a Main Stream architecture since the sample gas flows directly in the measuring chamber of the developed CO<sub>2</sub> sensor. A Heating system is implemented both on emitter and receiver stage, in order to avoid water vapor condensation. The Heating system is composed of resistances mounted on rear of the electronics boards that generates heat, an aluminum ring that surrounds the optical elements and conduce the generated heat along the measuring chamber, and a digital temperature sensor for the temperature monitoring. CPU controls the temperature of the emitter and the receiver stages by switching ON and OFF the current circulating in the resistances. A block diagram of the sensor and a drawing of the CO<sub>2</sub> section are reported in Figures 4 and 5.

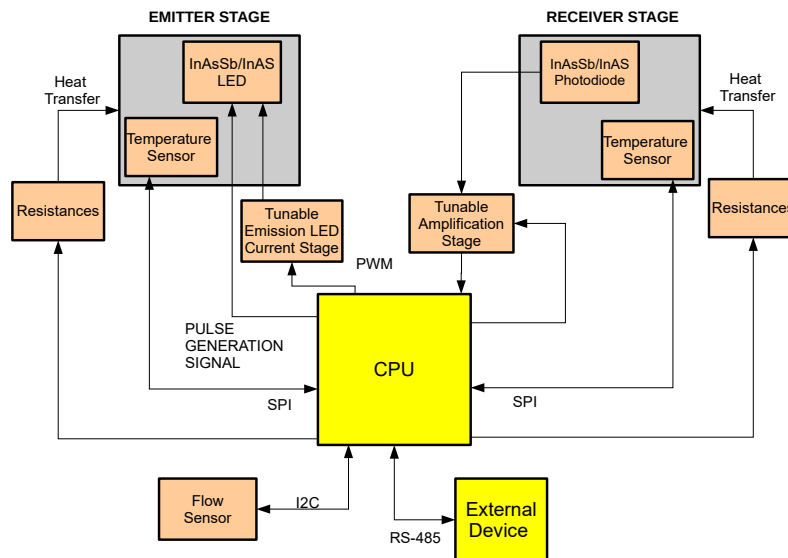


Figure 4. Schematic representation of the sensor.

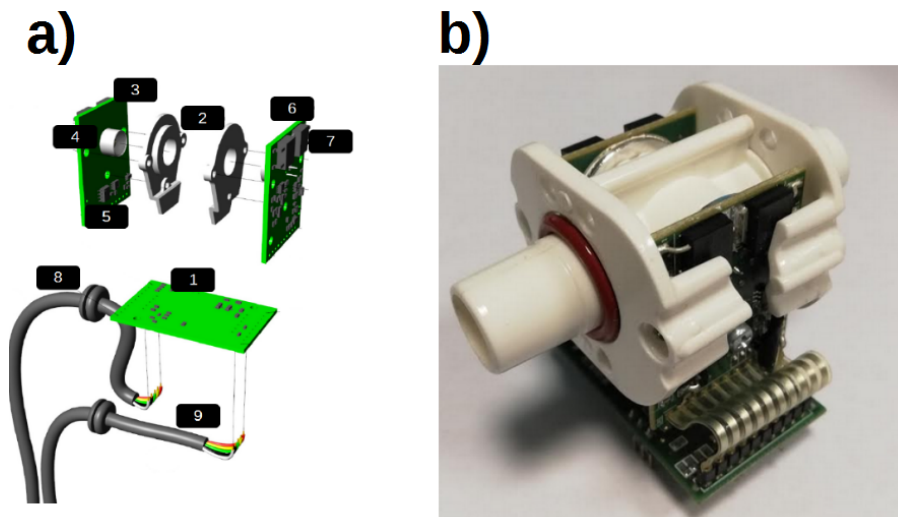


Figure 5. (a) Exploded drawing of the CO<sub>2</sub> sensor: (1) CPU board; (2) aluminum rings; (3) emitter board; (4) InAsSb/InAs element; (5) digital temperature sensor; (6) receiver board; (7) heating resistances; (8) Flow sensor communication cable; (9) power supply/RS-485 cable. (b) Assembly of the developed CO<sub>2</sub> and plastic cuvette.



Thanks to the implemented solution, the water vapor condensation is prevented not only directly on optical elements but also in their proximity, obtaining a water-free cuvette. Figure 6 shows an example of water vapor condensation on a cuvette placed at MO exhaust port that occurs without the implementation of a heating system, leading to a complete degradation of the optical signal.



**Figure 6.** Effect of water vapor condensation on a test cuvette placed at the exhaust port of a membrane oxygenator.

Further, in Figure 7 is reported the experimental result obtained recording optical signal from CO<sub>2</sub> sensors without the implemented heating system while relative humidity (RH%) of the gas flow increases. As RH% increases, water vapor starts to condensate on the measuring chamber walls and on optical elements, leading to signal degradation.

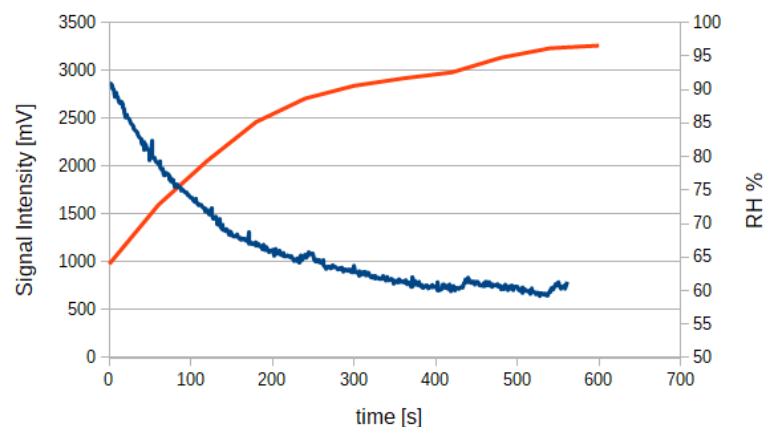


**Figure 7.** Optical signal intensity (blue) versus relative humidity (orange).

Gas temperature at the exhaust port of a MO usually is 38 °C during ECLS procedures such as CPB [31]; therefore, increasing the temperature of the sensor measuring chamber to 40 °C prevents water vapor condensation. Even though the heating of the sensor's measuring chamber prevents water vapor condensation, an increase in optical elements temperature brings side effects relevant to LED and PD efficiency. Moreover, the goal of the implemented heating system is to prevent water vapor condensation not only on optical elements but also on the entire measuring chamber, preventing formation of water drops that over time will move on the optical elements. For this reason, heating elements larger than the optical elements package has been used. This solution allows a more efficient diffusion of heat along the measuring chamber, preventing formation of water drops. Even if the above-mentioned solution is effective in preventing water drops formation on optical elements, it worsens the temperature control as larger oscillations in temperature on emitter and receiver stages are introduced. To correctly evaluate the effect of unstable temperature on LED and PD efficiency, preliminary both theoretical and experimental analysis have been carried out, and then a method to compensate the temperature effect has been proposed.

#### 2.4. Preliminary Analysis of Temperature Effect on Receiver Stage

Temperature increase of the receiver PD determines an increase of both dark current noise and response time. Dark current noise arises from the generation of a current on a photosensitive device even if photons are not detected. The movement of charges that generates the dark current noise mainly depends on the thermal condition of the device, and it increases as the temperature increases. This effect worsens the SNR (signal-to-noise ratio) but can be compensated through postprocessing on the acquired signal. Slower PD response can be compensated using an appropriately long for emission pulse, being sure that the pulse duration allows the PD to reach the steady-state. In our system, the emission pulses are generated at 100 Hz frequency with a pulse duration of 1 ms. To evaluate if the temperature affects the PD photosensitivity (i.e., the ability of the PD to generate current when hit by photons), a theoretical approach can be used. The spectral response of an InAsSb/InAs PD can be described by the sum of two Gaussian curves G1 and G2 [32]:

$$R_{PD}(\lambda, T) = R_0 \cdot [K_1 \cdot G_1(\lambda_{max}(T), \Delta\lambda(T)) + K_2 \cdot G_2(\lambda_{max}(T) - \lambda_0, \Delta\lambda_0)] \quad (3)$$

where  $R_0$  is the PD integral photodiode sensitivity [A/W],  $\Delta\lambda(T)$  is the FWHM,  $\lambda_{max}(T)$  is peak wavelength,  $K_1, K_2, \lambda_0$  and  $\Delta\lambda_0$  are adjustable parameters, set in order to fit the spectral response data provided by the manufacturer at  $T = 27^\circ\text{C}$  (Figure 8). As for the LED modeling:  $\Delta\lambda(T) \sim 0.1 \lambda_{max}(T)$  and  $d\lambda_{max}/dT = 4.5 \text{ nm}/^\circ\text{C}$  within the temperature range 0 to  $50^\circ\text{C}$ . Solving Equation (3) highlights that increase on PD temperature affects its photosensitivity only at high temperatures, whereas the effect on photosensitivity around  $40^\circ\text{C}$  can be considered negligible.

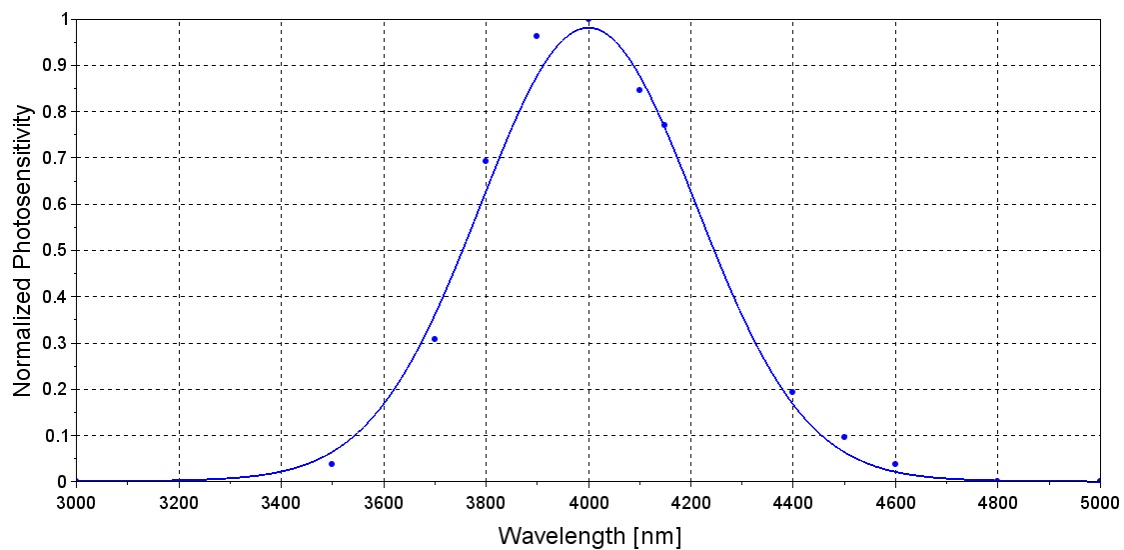


Figure 8. Simulated PD spectral response (solid line) and data provided by the manufacturer (dots) [30].

#### 2.5. Preliminary Analysis of Temperature Effect on the Emitter Stage

The following equation describes the emission of the mid-IR beam by an InAsSb/InAS LED,

$$P_{LED}(\lambda, T) = \frac{P_0}{\pi} \cdot \frac{\Delta\lambda(T)}{\Delta\lambda(T)^2 + (\lambda - \lambda_{max}(T))^2} \quad (4)$$

where  $P_0$  is the total output power [ $\mu\text{W}$ ],  $\lambda$  is the wavelength [nm],  $\Delta\lambda$  and  $\lambda_{max}$  are the FWHM (Full Width at Half Maximum) and peak wavelength of the emission spectra, respectively. For  $\lambda_{max}$  we considered the value provided by the LED datasheet at  $27^\circ\text{C}$  [30]. Within the temperature range 0 to  $50^\circ\text{C}$  the following relationships are valid,  $\Delta\lambda(T) \sim 0.1 \lambda_{max}(T)$  and  $d\lambda_{max}/dT = 4.5 \text{ nm}/^\circ\text{C}$  [32]. By solving Equation (4) is possible to describe the mid-IR LED emission spectra at



different temperatures. As the temperature increases, the peak wavelength of the emission spectra shifts to higher wavelengths values and at the same time the optical power intensity decreases, as reported in Figure 9 where the total output power of the LED was calculated in the temperature range 25 to 50 °C.

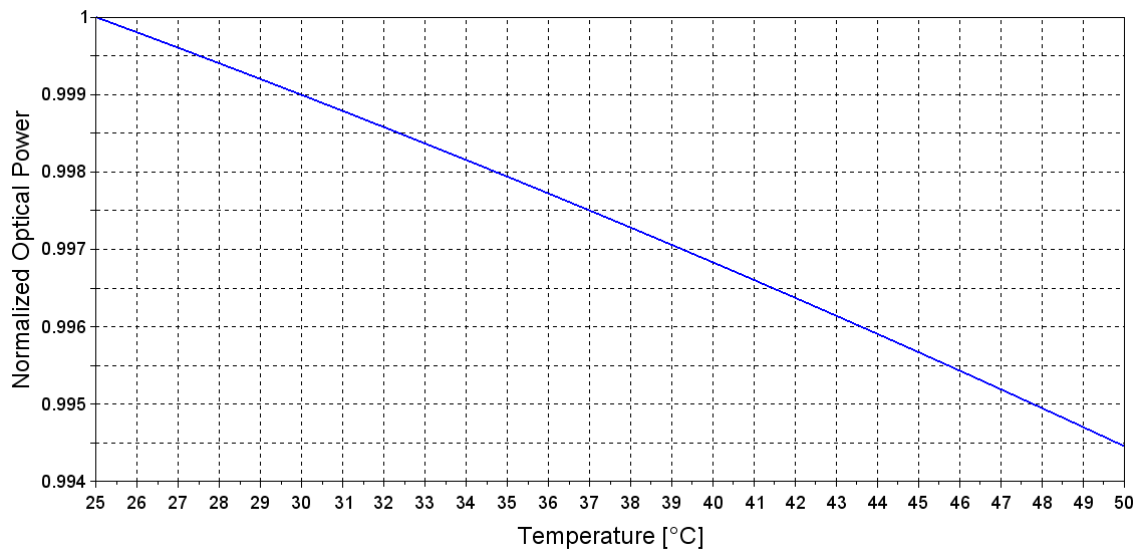


Figure 9. Theoretical evaluation of correlation between emitted optical power and temperature.

## 2.6. Experimental Analysis

Experimental analysis has been performed to validate the theoretical formulations reported in paragraphs 2.4 and 2.5. To experimentally evaluate the effect of temperature on the receiver element, sensor's output signal has been recorded activating the heating system only on the receiver stage, in order to avoid interference due to temperature effect on the emitter element. The theoretical formulation expressed by Equation (3) is confirmed experimentally (Figure 10), as we did not observe any correlation between the receiver stage temperature and the output sensor signal ( $R^2 = 0.02$ ). Therefore, the PD photosensitivity dependency on temperature is negligible in terms of optical signal variation and does not affect the measurement provided by our sensor.

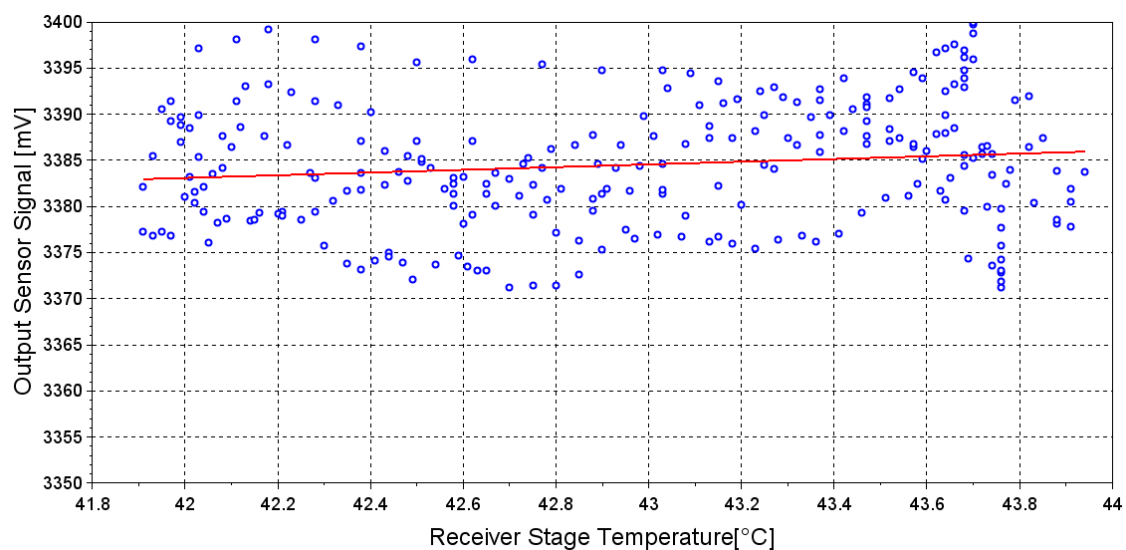
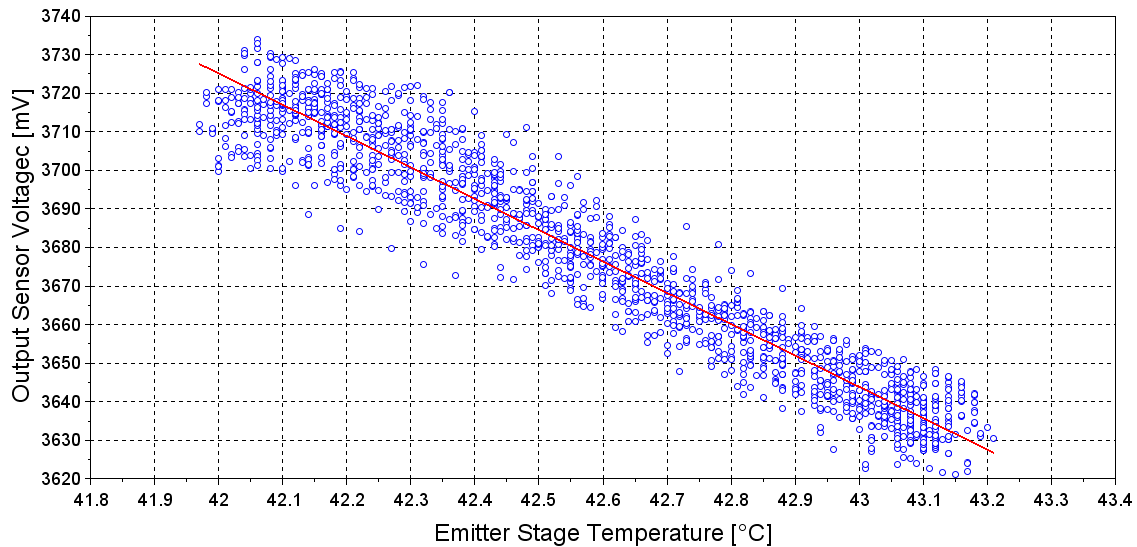


Figure 10. Experimental evaluation of correlation between emitted output power and receiver stage temperature. Blue dots represent the sampled value of the output sensor voltage at several temperatures of the receiver stage. Red line represents the linear regression of the data.

Effect of the temperature on the emitter element has been experimentally studied activating the heating system only on the emitter stage, acquiring the sensor output signal at several temperature values of the emitter stage. The experimental result (Figure 11), shows a negative linear correlation with an  $R^2$  coefficient of 0.93.



**Figure 11.** Experimental evaluation of correlation between emitted output power and emitter stage temperature. Blue dots represent the sampled value of the output sensor voltage at several temperatures of the emitter stage. Red line represents the linear regression of the data.

Anyway, even though Figures 9 and 11 both show a negative correlation between emitted optical power and temperature, their slopes are different. In particular, from the theoretical analysis the sensor signal variation due to temperature variation of the emitter element should be negligible, but this is not confirmed experimentally. This is because in theoretical formulation only the contribute of the LED is considered, while in the experiment is considered also the contribute of the receiver element. Therefore, to mathematically describe the effect of temperature variation on a single channel mid-IR sensor, both Emitter and Receiver spectral characteristics shall be considered. Equation (5) describes the sensor's optopair spectral characteristics [22].

$$A(\lambda, \lambda_{max}(T)) = P_{LED}(\lambda, T) \cdot R_{PD}(\lambda, T) \quad (5)$$

Solving equation (5) for the Emitter temperature range 42 to 43 °C and considering PD temperature at 27 °C, allows to simulate the experiment of Figure 11. The result reported in Figure 12 shows that increase of 1 °C reduces the output of 1.5%, while in the experiment of Figure 11 increase of 1 °C reduces the output of 2%. Considering the approximation made by the mathematical model, this result confirm that the theoretical formulation correctly describe the behaviour observed experimentally.

This result confirm that the proposed formulation is suitable for describing the behaviour of a single channel optical sensor.

From the experiment we estimated that the sensor output signal decreases of approximately 70 mV/°C. Considering that in our sensor, the output signal is reduced by approximately 700 mV at maximum measurable value of CO<sub>2</sub> concentration, and considering the non-linearity of the sensor response described by (2), the above mentioned signal–temperature variability can not be tolerated. Further, a signal decrease due to LED temperature increase was noticed even if the heating system was turned off, due to "self-heating" of the LED. The current circulating in the LED is indeed sufficient to increase the temperature of the optical element, thus affecting its emitted power as discussed before. Therefore, a strategy to avoid the sensor signal variation due to the temperature variation at the

emitter stage is necessary. Such strategy to achieve the signal stability is described in detail in the following paragraphs.

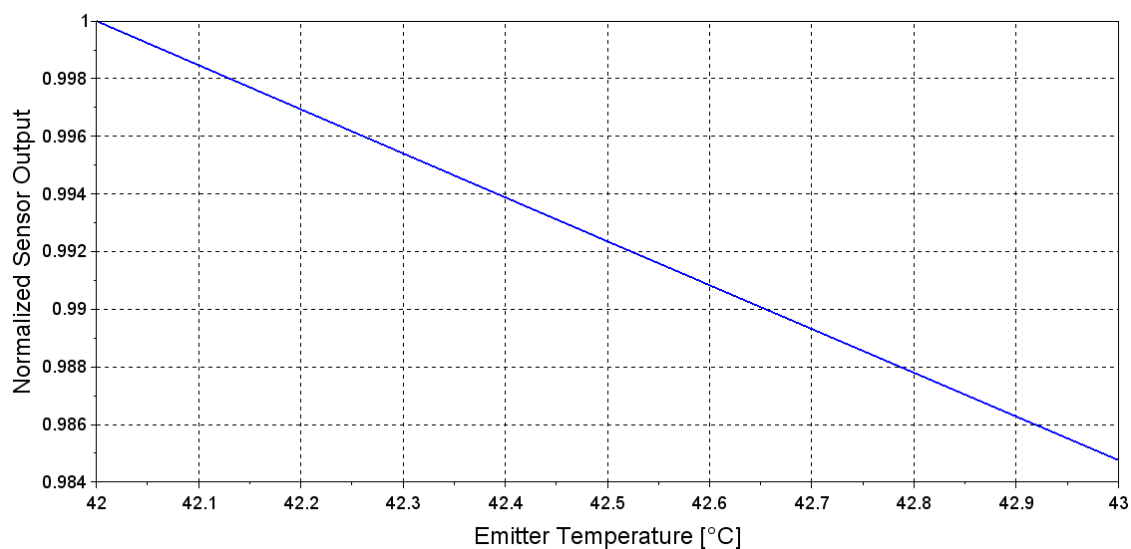


**Figure 12.** Theoretical evaluation of correlation between sensor's output and emitter element temperature, using sensor optopair formulation.

### 2.7. Temperature Control Algorithm

The results of the preliminary analysis suggest that temperature variations on the emitter stage represent the major contributor to output sensor signal variation, whereas the temperature effect on the sensitivity of the receiver can be considered negligible. Therefore, a method to compensate the temperature variations on the emitter stage was studied, in order to improve the output signal stability. The proposed method consists of an algorithm for the generation of periodical and controlled temperature variations on the emitter stage, and synchronization of the optical signal acquisition at known temperature conditions. In this way, the optical signal is always sampled at the same thermal conditions, and the signal variations due to heating-cooling dynamics are not taken into account. The developed algorithm is made of two phases:

- an initial phase performed at start-up, necessary to allow the sensor to reach the steady state temperature, and
- a phase in which the heating module is alternatively turned on and off by the CPU.

The initial phase (FIND\_T\_REG state) is necessary to tune the control algorithm on the room temperature and to assure repeatability of the generated temperature oscillations used in the second phase. During the second phase, the CPU generates controlled temperature oscillations switching alternatively on and off the heating system. The heating system is switched off when the emitter stage temperature reaches a threshold value (HeaterRefT) based on the steady state temperature. While the heating system is turned off (ACQ\_NO\_HEATING state) the output signal is acquired and processed by the CPU through a moving average filter. This condition is maintained for a fixed duration of 45 s. Once the 45 s elapse the algorithm moves to the WAIT\_COOLING state in which the signal acquisition is stopped and the sensor output signal is no more updated. During this state the heating system is maintained off until a threshold value is reached (HeaterRefT - HYST\_TEMP\_HEATER\_OFF). Further, in this state, also the emitter LED is turned off in order to remove the LED self-heating due to electrical current circulating. Once reached the threshold value, the algorithm moves to the HEATING\_NO\_ACQ state in which both the LED and heating system are turned on again. The algorithm then continues cyclically. A schematic representation of the algorithm is reported in Figure 13.

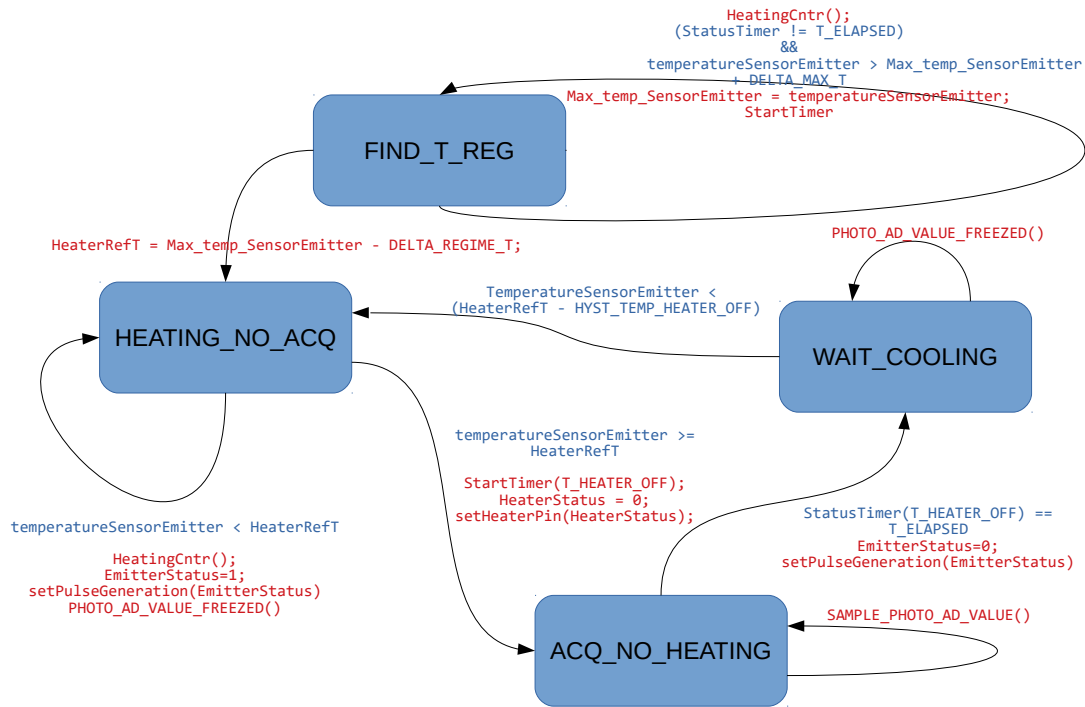


Figure 13. State diagram of Temperature Control Algorithm.

Through the proposed algorithm, the sensor output signal is updated only at the same thermal conditions, therefore the output changes due to temperature variation are avoided. In Figure 14 the emitter stage temperature trend over time with the proposed control algorithm is reported, while Figure 15 reports the sensor output signal obtained from the algorithm.

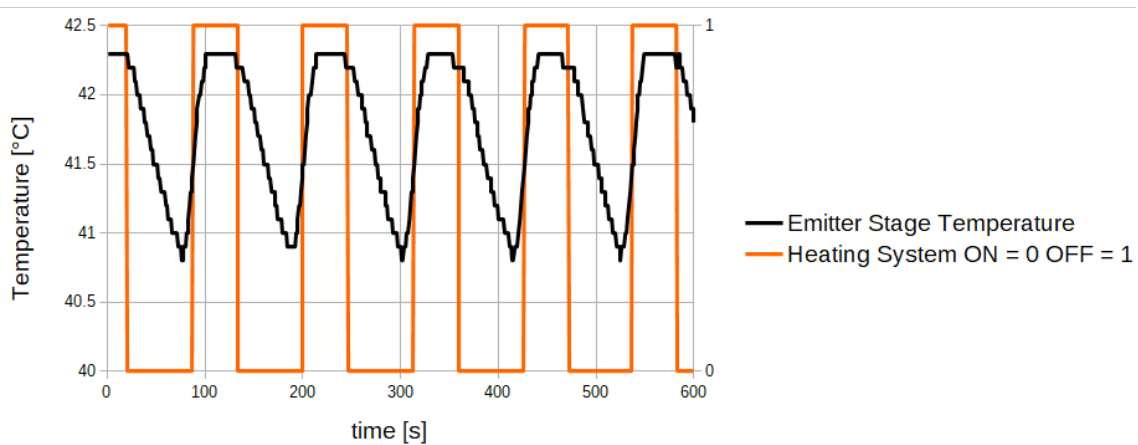
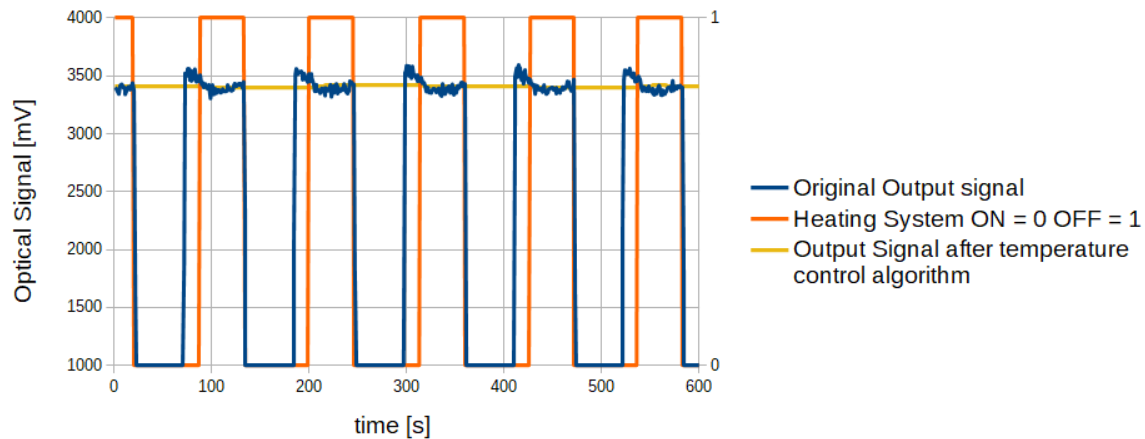


Figure 14. Emitter Stage Temperature trend obtained through the temperature control algorithm.

As shown in Figure 14, the emitter stage temperature reaches the same values at each acquisition cycle (HEATING\_NO\_ACQ state). Therefore, as reported in Figure 15, the output signal obtained through averaging operation of the signal acquired during the HEATING\_NO\_ACQ state is much more stable than the original signal. Without the implementation of the proposed algorithm, temperature dynamics on the emitter stage is characterized by oscillations without a defined period. Therefore, the use of simple filtering methods such as a moving average on the acquired signal result poorly effective as the temperature–signal dependency remains.



**Figure 15.** Original output signal (blue) and output signal (yellow) obtained through the temperature control algorithm.

### 3. Results

#### 3.1. Sensor Validation in Experimental Laboratory Setting

The developed CO<sub>2</sub> sensor and temperature control algorithm was tested in terms of CO<sub>2</sub> measurement accuracy. Before testing, the sensor was calibrated by using gas tanks containing gas mixtures of air and CO<sub>2</sub> with known concentrations. The measurement range for CO<sub>2</sub> concentration was 0–9%, as the developed sensor is intended to be used for treating patients in hypercapnic conditions (i.e., P<sub>a</sub>CO<sub>2</sub> higher than 50 mmHg [33], corresponding to a CO<sub>2</sub> concentration of approximately 6.5%). The gas was let flow through the sensor and the output signal was recorded through a PC connected to the sensor via RS-485 communication line. The following CO<sub>2</sub> concentrations were used for the calibration procedure; 0%, 2.5%, 5%, 7.5%, and 9%. The collected data were used to obtain a calibration curve through polynomial interpolation (Figure 16).

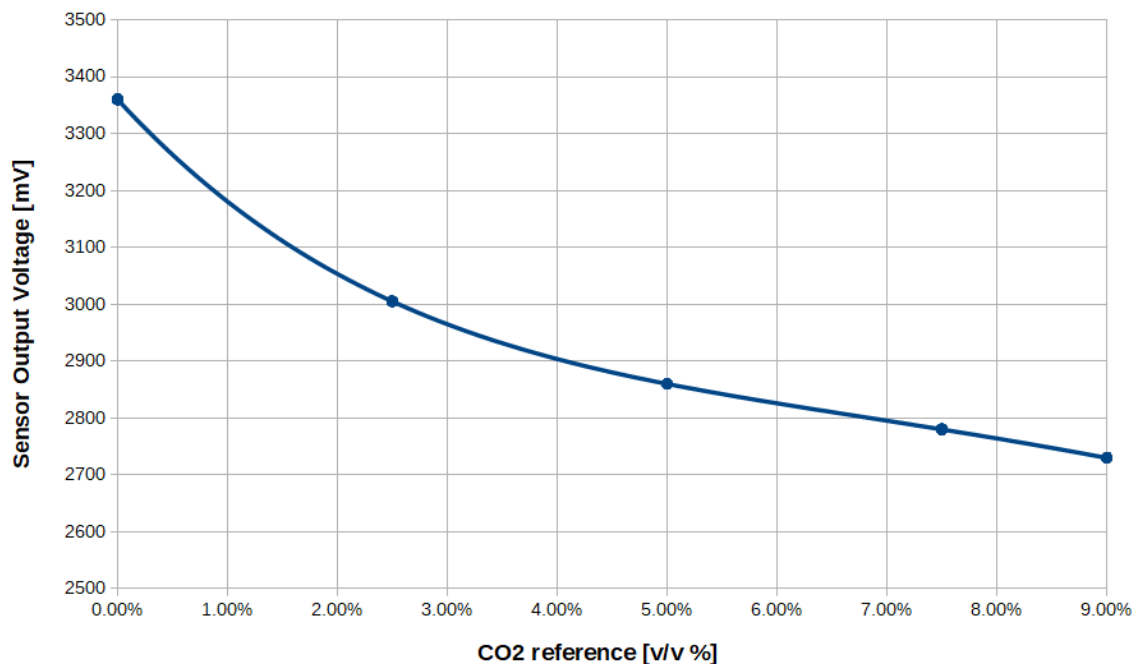


**Figure 16.** Example of calibration curve. Dots represent the values used for polynomial interpolation.

The parameters that define the calibration curve were then loaded in the CO<sub>2</sub> sensors. Sensor accuracy was verified by comparing its measurement with the ones obtained by a “gold standard”

device (Medtronic Microcap Plus Capnograph). The accuracy of the two sensors was compared using a mixture of air and CO<sub>2</sub> at several concentrations. In order to control the CO<sub>2</sub> concentration of the gas mixture used for the test, it was analyzed through a bench gas analyser (Servomex MiniMP 5200). Test results are reported in Figure 17.

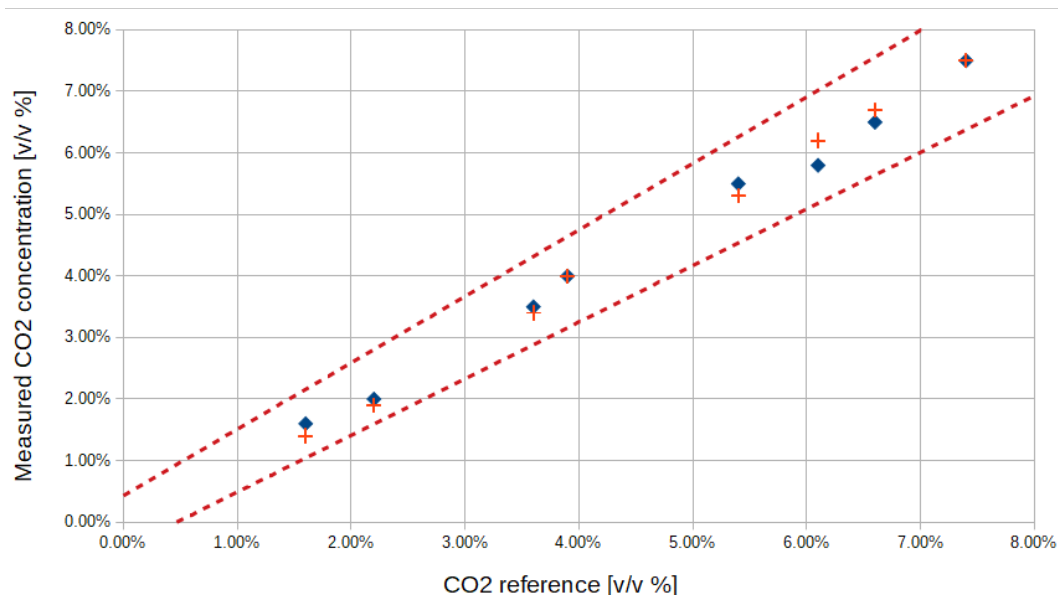


**Figure 17.** CO<sub>2</sub> concentration measurement provided by the newly developed sensor (blue diamonds) and by the “gold standard” device (orange crosses). Dashed lines represent the ISO 80601-2-55 error limits.

From data reported in Table 1, the average absolute error obtained for the newly developed sensor (0.13%) is similar to the one obtained by the reference device (0.15%), that is already validated for clinical practice. Further, the accuracy level shown by the new sensor complies with requirements prescribed by ISO 80601-2-55. These results demonstrate the efficiency of the temperature control algorithm in terms of output signal stability, therefore the reliability of the newly developed sensor.

**Table 1.** Comparison between measurements get by the developed sensor and a “gold standard” device for several CO<sub>2</sub> concentration values. Error is expressed as average value and standard deviation (SD).

CO <sub>2</sub> Concentration Set-Point [v/v %]	Developed CO <sub>2</sub> Sensor	“Gold Standard” Sensor
1.60 %	1.60 %	1.40 %
2.20 %	2.00 %	1.90 %
3.60 %	3.50 %	3.40 %
3.90 %	4.00 %	4.00 %
5.40 %	5.50 %	5.30 %
6.10 %	5.80 %	6.20 %
6.60 %	6.50 %	6.70 %
7.40 %	7.50 %	7.50 %
Average Error ± SD	0.13 ± 0.09%	0.15 ± 0.07 %

### 3.2. In Vivo Sensor Validation

To validate the new device in vivo, we tested the sensor in an animal model, and compared the obtained measurements with the ones taken with Medtronic Microcap Plus Capnograph. Data were collected during the execution of experiments described in [7], in which pigs with induced cardiogenic shock were undergoing ECMO procedure. Measurements from the newly developed capnometer and the reference device were taken at the MO exhaust port. Further, the GF measurement taken at



the inlet port of the MO through our flow sensor and the one provided by a reference device were compared. Finally,  $VCO_2$  data obtained by  $CO_2$  measurement from our system were evaluated against  $VCO_2$  calculated through data gathered by the reference device. Both for the newly developed sensor and reference device the following formula was used for determination of  $VCO_2$ ,

$$VCO_2(mL/min) = \frac{GF(mL/min) \cdot CO_2\%}{100} \quad (6)$$

As during in vivo tests the  $CO_2$  concentration cannot be set, to validate our sensor we focused on the error obtained comparing the measurements from our sensor with the ones taken with the reference device, that is routinely used in clinical practice. Results are reported in Table 2.

**Table 2.** Error between measurement taken with the newly developed system and the “gold standard” devices for  $CO_2$  concentration, Gas Flow, and  $VCO_2$ . Error is expressed as average value and standard deviation (SD).

Gas Flow Developed Sensor [L/min]	Gas Flow “Gold Standard” Sensor [L/min]	$CO_2$ Concentration Developed Sensor [v/v %]	$CO_2$ Concentration “Gold Standard” Sensor [v/v %]	$VCO_2$ Developed Sensor [mL/min]	$VCO_2$ “Gold Standard” Sensor [mL/min]
1.60	1.50	3.80 %	3.80 %	60.8	57.0
1.00	1.00	7.00 %	6.90 %	70.0	69.0
1.00	1.00	7.10 %	7.00 %	71.0	70.0
1.10	1.00	8.20 %	8.30 %	90.2	83.0
1.50	1.40	7.60 %	7.60 %	114.0	106.4
2.20	2.10	5.20 %	5.00 %	114.4	105.0
3.60	3.60	3.60 %	3.40 %	129.6	122.4
0.80	0.70	5.00 %	4.80 %	40.0	33.6
3.10	3.00	4.40 %	4.40 %	136.4	132.0
4.50	4.50	3.60 %	3.40 %	162.0	153.0
Gas Flow Average Error $\pm$ SD [L/min]		$CO_2$ Concentration Average Error $\pm$ SD [v/v %]		$VCO_2$ Average Error $\pm$ SD [mL/min]	
0.06 $\pm$ 0.05		0.11 $\pm$ 0.09		5.7 $\pm$ 3	

These results show that the newly developed  $CO_2$  sensing system represents a reliable solution in the clinical environment. Based on the results obtained both in vitro and in clinical environment, the developed sensor has obtained the CE mark and it is currently used in intensive care units connected to multiparametric monitoring systems for ECMO procedures and to ECCO2R devices.

#### 4. Discussion and Conclusions

In this paper, we present a new sensor specifically designed for measurement of carbon dioxide concentration in the exhaust gas of a membrane oxygenator during extracorporeal procedures. The developed sensor is made up by two sections: one for measurement of the gas flow applied to a membrane oxygenator, and the other for the measurement of carbon dioxide concentration in the exhaust gas, which represents the  $CO_2$  removed from the patient’s blood. The proposed  $CO_2$  sensor is designed as a Main Stream sensor with a single channel optical architecture, avoiding use of optical filters and therefore obtaining a simple, cheap and easy to assemble system. As the oxygenator exhaust gas is characterized by an high amount of water vapor, condensation at the exhaust connector is easy to occur. Therefore, in order to avoid water vapor condensation within the optical sensor, with consequent degradation of the optical signal, a heating module is implemented in the  $CO_2$  measurement section. Even though the implemented heating system prevents water vapor condensation, temperature variations affect the performance of the optical elements. Temperature effect on the optical elements used in the  $CO_2$  sensor was analyzed both theoretically and experimentally, highlighting the strong correlation between emitter LED temperature and acquired optical signal. Even though both theoretical evaluation and experimental results highlight a negative correlation between emitted optical power and emitter stage temperature, reported in Figures 8 and 11, respectively, the two relationship are characterized by different slopes. This result can be explained considering that, in the experimental setup, the sensor photodiode contributes to the variation of sensor’s output, while in equation (4) this contribute is not taken into account. To correctly describe the experimental

setup, the formulation reported in equation (5) has been used. This formulation considers both the emitter and receiver contribute to the sensor output. Using it to simulate the experimental setup the obtained relationship between sensor output and emitter temperature (shown in Figure 12) is close to the one obtained experimentally (Figure 11). The mathematical model used was confirmed valid and useful to evaluate the effect of temperature changes introduced by the heating system of our device on the optical elements. Further, as reported in [32], the mathematical modeling can be also used to evaluate sensor sensitivity. Therefore, the adopted mathematical model represents the basis for further improvement of our device since allows to explore the behavior of our sensor for different conditions of use, e.g., higher temperatures, different optical path length, and higher CO<sub>2</sub> concentration. In order to remove the signal–temperature dependency and therefore improve sensor sensitivity, an algorithm for heating system control was implemented. The proposed solution consists in the generation of controlled and repeatable temperature oscillations and acquisition of the sensor's output signal always at the same thermal conditions. Use of the proposed temperature control algorithm, results in a stable output signal since only samples acquired at the same thermal conditions are considered. The main drawback of the implemented solution is the low time resolution of the measurement. Considering the duration of a thermal cycle, there is a 90 seconds delay in the detection of a CO<sub>2</sub> concentration variation. Anyway, we do not consider this a major problem considering that the sensor is intended for long term therapy that lasts for days or weeks, meaning that the data gathered through the sensors are used to get long-term information about therapy progress and trends. Accuracy of the developed sensor has been compared against a CO<sub>2</sub> sensor used in clinical practice both through laboratory test and in vivo test. The results suggest that the developed system allows a reliable measurement of gas flow and carbon dioxide concentration, and therefore of carbon dioxide removal rate VCO<sub>2</sub>. Is important to highlight that, the reference device considered as gold standard in our experiments is a CO<sub>2</sub> sensor intended for respiratory monitoring, and it is able to perform the measurements only in "intermittent" gas flow conditions like breathing. Therefore, during our experiments the reference device was manually connected/disconnected from the MO exhaust port. This means that sensors designed for respiratory monitoring, like the one used as gold standard in our experiments, are not suitable for use in ECLS procedure due the impossibility of measurement in continuous gas flow conditions. As far as the author knows, only another device for measuring of CO<sub>2</sub> concentration specifically designed for ECLS application is available at the moment, the CO<sub>2</sub> sensor of Spectrum M4 system (Spectrum Medical, Gloucester, England), but no information about its functioning or its performances in terms of CO<sub>2</sub> concentration accuracy was found nor it was possible to compare this device with our sensor experimentally. The developed sensor fulfills the requirements prescribed by ISO 80601-2-55 standard relevant to the accuracy of measurements of carbon dioxide concentration and has already obtained the CE mark. It is currently in use in intensive care units connected to multi-parametric monitoring systems for ECMO procedures and to ECCO<sub>2</sub>R devices. From the feedback obtained through clinical practice, a more deep validation will be performed.

**Author Contributions:** Conceptualization, M.B. and G.C.; methodology, M.B. and L.C.; software, M.B. and G.C.; writing—original draft, M.B. and L.C.; writing—review and editing, M.B, L.C. and E.M.; supervision, S.S. and E.M. All authors have read and agreed to the published version of the manuscript.

**Funding:** This research was sponsored by MediCon Ingegneria srl.

**Acknowledgments:** The authors would like to thank Eurosets s.r.l. for providing equipment for the laboratory test and data for the in vivo test.

**Conflicts of Interest:** L.C., S.S. and E.M. declare no conflict of interest. M.B. is a full-time employee at MediCon Ingegneria s.r.l., in the framework of a PhD Apprenticeship Program at University of Bologna, G.C. is Technical Director and Co-Owner of MediCon Ingegneria s.r.l.

## References

1. Davis, D.P. Quantitative capnometry as a critical resuscitation tool. *J. Trauma Nurs.* **2005**, *12*, 40. [[CrossRef](#)] [[PubMed](#)]

2. Cereceda-Sánchez, F.J.; Molina-Mula, J. Systematic Review of Capnography with Mask Ventilation during Cardiopulmonary Resuscitation Maneuvers. *J. Clin. Med.* **2019**, *8*, 358. [CrossRef]
3. Eipe, N.; Doherty, D.R. A review of pediatric capnography. *J. Clin. Monit. Comput.* **2010**, *24*, 261–268. [CrossRef] [PubMed]
4. Grmec, Š. Comparison of three different methods to confirm tracheal tube placement in emergency intubation. *Intensive Care Med.* **2002**, *28*, 701–704. [CrossRef] [PubMed]
5. Kupnik, D.; Skok, P. Capnometry in the prehospital setting: Are we using its potential? *Emergency Med. J.* **2007**, *24*, 614–617. [CrossRef]
6. Baraka, A.; El-Khatib, M.; Muallem, E.; Jamal, S.; Haroun-Bizri, S.; Aouad, M. Oxygenator exhaust capnography for prediction of arterial carbon dioxide tension during hypothermic cardiopulmonary bypass. *J. Extra-Corporeal Technol.* **2005**, *37*, 192.
7. Montalti, A.; Belliato, M.; Gelsomino, S.; Nalon, S.; Matteucci, F.; Parise, O.; de Jong, M.; Makhoul, M.; Johnson, D.M.; Lorusso, R. Continuous monitoring of membrane lung carbon dioxide removal during ECMO: Experimental testing of a new volumetric capnometer. *Perfusion* **2019**, *34*, 538–543. [CrossRef] [PubMed]
8. Duscio, E.; Cipulli, F.; Vasques, F.; Collino, F.; Rapetti, F.; Romitti, F.; Behnemann, T.; Niewenhuys, J.; Tonetti, T.; Pasticci, I.; et al. Extra-corporeal CO<sub>2</sub> removal: The minimally invasive approach, theory, and practice. *Crit. Care Med.* **2019**, *47*, 33–40. [CrossRef] [PubMed]
9. Epis, F.; Belliato, M. Oxygenator performance and artificial-native lung interaction. *J. Thoracic Dis.* **2018**, *10*, S596. [CrossRef] [PubMed]
10. Potger, K.C.; McMillan, D.; Southwell, J.; Dando, H.; O Shaughnessy, K. Membrane oxygenator exhaust capnography for continuously estimating arterial carbon dioxide tension during cardiopulmonary bypass. *J. Extra-Corporeal Technol.* **2003**, *35*, 218–223.
11. Bembea, M.M.; Lee, R.; Masten, D.; Kibler, K.K.; Lehmann, C.U.; Brady, K.M.; Easley, R.B. Magnitude of arterial carbon dioxide change at initiation of extracorporeal membrane oxygenation support is associated with survival. *J. Extra-Corporeal Technol.* **2013**, *45*, 26.
12. Morales-Quinteros, L.; Del Sorbo, L.; Artigas, A. Extracorporeal carbon dioxide removal for acute hypercapnic respiratory failure. *Ann. Intensive Care* **2019**, *9*, 79. [CrossRef]
13. Msimo EMMA Capnometer Datasheet. Available online: [https://www.masimo.com/siteassets/us/documents/pdf/plm-10642a\\_product\\_information\\_emma\\_capnograph\\_us.pdf](https://www.masimo.com/siteassets/us/documents/pdf/plm-10642a_product_information_emma_capnograph_us.pdf) (accessed on 20 November 2019).
14. Medtronic Microcap Capnometer Datasheet. Available online: <https://www.medtronic.com/covidien/en-us/products/capnography/microcap-handheld-capnographs.html> (accessed on 20 November 2019).
15. Hodgkinson, J.; Tatam, R.P. Optical gas sensing: A review. *Meas. Sci. Technol.* **2012**, *24*, 012004. [CrossRef]
16. Stuart, B. Infrared spectroscopy. *Kirk-Othmer Encycl. Chem. Technol.* **2000**, 1–18. [CrossRef]
17. Dinh, T.V.; Choi, I.Y.; Son, Y.S.; Kim, J.C. A review on non-dispersive infrared gas sensors: Improvement of sensor detection limit and interference correction. *Sens. Actuators, B* **2016**, *231*, 529–538. [CrossRef]
18. Bezyazychnaya, T.; Bogdanovich, M.; Kabanov, V.; Kabanau, D.; Lebiadok, Y.; Parashchuk, V.; Ryabtsev, A.; Ryabtsev, G.; Shpak, P.; Shchemelev, M.; et al. Light emitting diode–photodiode optoelectronic pairs based on the InAs/InAsSb/InAsSbP heterostructure for the detection of carbon dioxide. *Semiconductors* **2015**, *49*, 980–983. [CrossRef]
19. Gordon, I.E.; Rothman, L.S.; Hill, C.; Kochanov, R.V.; Tan, Y.; Bernath, P.F.; Birk, M.; Boudon, V.; Campargue, A.; Chance, K.; et al. The HITRAN2016 molecular spectroscopic database. *J. Quant. Spectrosc. Radiat. Transfer* **2017**, *203*, 3–69. [CrossRef]
20. Degner, M.; Jürß, H.; Ewald, H. Fast and low power optical CO<sub>2</sub>-sensors for medical application: New sensor designs for main-and side-stream CO<sub>2</sub>-sensors are presented in comparison with state of the art capnometers. In Proceedings of the 2018 IEEE International Instrumentation and Measurement Technology Conference (I2MTC), Houston, TX, USA, 14–17 May 2018; pp. 1–5.
21. Jaffe, M.B. Infrared measurement of carbon dioxide in the human breath: “breathe-through” devices from Tyndall to the present day. *Anesthesia Analgesia* **2008**, *107*, 890–904. [CrossRef] [PubMed]
22. Sotnikova, G.Y.; Gavrilov, G.A.; Aleksandrov, S.E.; Kapralov, A.A.; Karandashev, S.A.; Matveev, B.A.; Remenny, M.A. Low Voltage CO<sub>2</sub>-Gas Sensor Based on III–V Mid-IR Immersion Lens Diode Optopairs: Where we Are and How Far we Can Go? *IEEE Sens. J.* **2009**, *10*, 225–234. [CrossRef]

23. Walsh, B.K.; Crotwell, D.N.; Restrepo, R.D. Capnography/Capnometry during mechanical ventilation: 2011. *Respir. Care* **2011**, *56*, 503–509. [CrossRef] [PubMed]
24. ISO—International Organization for Standardization. ISO 80601-2-55 Medical Electrical Equipment—Particular Requirements for the Basic Safety and Essential Performance of Respiratory Gas Monitors. Available online: [https://infostore.saiglobal.com/preview/98695750340.pdf?sku=867463\\_saig\\_nsai\\_nsai\\_2063036](https://infostore.saiglobal.com/preview/98695750340.pdf?sku=867463_saig_nsai_nsai_2063036) (accessed on 26 June 2020).
25. Capnometer. Available online: <https://patentimages.storage.googleapis.com/f9/f3/7a/67700280bd19d5/WO2016092308A1.pdf> (accessed on 26 June 2020).
26. Jaffe, M.B. Mainstream or sidestream capnography? *Environment* **2002**, *4*, 5.
27. Aittomäki, J. Monitoring of CO<sub>2</sub> exchange during cardiopulmonary bypass: the effect of oxygenator design on the applicability of capnometry. *Perfusion* **1993**, *8*, 337–344. [CrossRef] [PubMed]
28. Høgetveit, J.O.; Kristiansen, F.; Pedersen, T.H. Development of an instrument to indirectly monitor arterial pCO<sub>2</sub> during cardiopulmonary bypass. *Perfusion* **2006**, *21*, 13–19. [CrossRef] [PubMed]
29. Kim, S.J.; Jang, S.P. Experimental and numerical analysis of heat transfer phenomena in a sensor tube of a mass flow controller. *Int. J. Heat Mass Transfer* **2001**, *44*, 1711–1724. [CrossRef]
30. LED MicrosensorNT: LED and Photodiode Datasheet. Available online: <http://lmsnt.com/> (accessed on 20 November 2019).
31. Kristiansen, F.; Høgetveit, J.O.; Pedersen, T.H. Clinical evaluation of an instrument to measure carbon dioxide tension at the oxygenator gas outlet in cardiopulmonary bypass. *Perfusion* **2006**, *21*, 21–26. [CrossRef] [PubMed]
32. Aleksandrov, S.; Gavrilov, G.; Kapralov, A.; Matveev, B.; Sotnikova, G.Y.; Remennyi, M. Simulation of characteristics of optical gas sensors based on diode optopairs operating in the mid-IR spectral range. *Tech. Phys.* **2009**, *54*, 874–881. [CrossRef]
33. del Castillo, J.; López-Herce, J.; Matamoros, M.; Cañadas, S.; Rodríguez-Calvo, A.; Cechetti, C.; Rodríguez-Núñez, A.; Álvarez, A.C.; Iberoamerican Pediatric Cardiac Arrest Study Network RIBEPCL. Hyperoxia, hypocapnia and hypercapnia as outcome factors after cardiac arrest in children. *Resuscitation* **2012**, *83*, 1456–1461. [CrossRef]



© 2020 by the authors. Licensee MDPI, Basel, Switzerland. This article is an open access article distributed under the terms and conditions of the Creative Commons Attribution (CC BY) license (<http://creativecommons.org/licenses/by/4.0/>).